Cellulose (2012) 19:1631–1643
DOI 10.1007/s10570-012-9745-x

ORIGINAL PAPER

Morphological development of cellulose fibrils of a bleached eucalyptus pulp by mechanical fibrillation

Q. Q. Wang · J. Y. Zhu · R. Gleisner · T. A. Kuster · U. Baxa · S. E. McNeil

Received 25 April 2012/Accepted 11 July 2012/Published online: 25 July 2012

Abstract This study reports the production of cellulose nanofibrils (CNF) from a bleached eucalyptus pulp using a commercial stone grinder. Scanning electronic microscopy and transmission electronic microscopy imaging were used to reveal morphological development of CNF at micro and nano scales, respectively. Two major structures were identified (1) highly kinked, naturally helical, and untwisted fibrils that serve as backbones of CNF networks, and (2) entangled, less distinctively kinked (or curled) and twisted "soft looking" nanofibrils. These two major structures appeared in different features of CNF network such as "trees", "net", "flower", single fibril, etc. Prolonged fibrillation can break the nanofibrils into nanowhiskers from the untwisted fibrils with high crystallinity. Energy input for mechanical fibrillation is on the order of 5–30 kWh/kg. The gradual reduction in network size of CNF with time may be used to fractionate CNF.

Keywords Cellulose nanofibrils (CNF) Morphology · Mechanical fibrillation/grinding · Fiber/fibril network · TEM imaging · Nanowhisker

This work was conducted on official government time of Zhu, Gleisner, and Kuster. Wang was a visiting student at the USDA Forest Service, Forest Products Laboratory.

Q. Q. Wang
State Key Lab of Pulp and Paper Engineering, South China University of Technology, Guangzhou, China

J. Y. Zhu (✉) · R. Gleisner · T. A. Kuster
Forest Products Laboratory, USDA Forest Service, Madison, WI, USA
e-mail: jzhu@fs.fed.us

U. Baxa
Electron Microscopy Laboratory, Advanced Technology Program, SAIC-Frederick Inc., NCI-Frederick, Frederick, MD 21702, USA

S. E. McNeil
Nanotechnology Characterization Laboratory, Advanced Technology Program, SAIC-Frederick Inc. NCI-Frederick, Frederick, MD 21702, USA

Introduction

Cellulose accounts for approximately 40% of lignocellulosic biomass and can be used for a variety of applications. As a structural material, cellulose is very strong and has a very strong tensile strength (Wegner and Jones 2009). It has been demonstrated that using nanocellulose, an elemental building block of cellulose, can produce a variety of high performance new materials and products from the bottom up (Eichhorn et al. 2010; Habibi et al. 2010; Klemm et al. 2011; Sir6 and Plackett 2010). However, the utility of nanocellulose has not been well recognized by the broad scientific community. Major research efforts are primarily conducted by traditional wood utilization institutions throughout the world.

Lignocelluloses have a hierarchical structure and are a composite of cellulose, hemicelluloses, and lignin. Separating cellulose into its elemental form of nanofibrils, approximately 3–20 nm in width, is a difficult task. Mechanical nanofibrillation of bleached pulp has been successful in producing cellulose nanofibrils (CNF) using high pressure homogenizers pääkkö et al. 2007; Siró et al. 2011; Turbak et al. 1983), minofluidizers (Henriksson et al. 2008; Zhu et al. 2011), and grinders (Iwamoto et al. 2008; Iwamoto et al. 2007). However, mechanical fibrillation is very energy intensive. A fundamental understanding of the morphological development of cellulosic fibers during nanofibrillation can help to develop effective strategies for process improvement and facilitate fibrillation to reduce energy consumption. Furthermore, morphological properties of cellulose nanofibrils are important to a variety of applications, such as polymer reinforcement and nanofiber production through electrospinning. Depending on the fibrillationprocess and any pretreatment step adopted before mechanical fibrillation, the morphology of the resultant CNF can be very different. For example, TEMPO-mediated oxidation pretreatment can result in a relatively uniform network of nanofibrils (Saito et al. 2009). The sizes and structures of nanofibril networks are affected by not only whether or not a particular pretreatment is applied before nanofibrillation, but they can also be affected by the degree of fibrillation, feedstock species, etc. Softwood pulps have been extensively used for CNF production (Henriksson et al. 2008; Iwamoto et al. 2007; Nakagaito and Yano 2004; Tejado et al. 2012; Uetani and Yano 2011 ; Zimmermann et al. 2004). Softwood species have relatively simple cell wall structures (e.g., absent of vessels as in hardwoods), and relatively uniform nanofibrils (Iwamoto et al. 2007) and morphology (Stelte and Sanadi 2009) were produced through mechanical fibrillation with less mechanical milling than used for hardwoods to produce equivalent fibrillations (Stelte and Sanadi 2009). Hardwood species are known to have a more rigid structure than softwoods due to their high Runkel ratio (cell wall thickness divided by lumen radius). Extensive mechanical fibrillation is required to open the spirally layered S1 secondary wall to access the inner S2 layer (Law et al. 1985; Marton et al. 1979) to facilitate CNF production. Therefore, morphological development of hardwood cellulose for CNF production is interesting; however, limited studies were conducted, especially under extensive fibrillation conditions.

The objective of this study is to conduct an examination of the morphologies of cellulose nanofibrils produced through direct mechanical fibrillation using a bleached hardwood eucalyptus kraft pulp. Kraft bleached pulp is less expensive and has a higher hemicellulose content than dissolving pulp used in many literature studies (Henriksson et al. 2008; Iwamoto et al. 2007; Stelte and Sanadi 2009). Fibrillation was extended much longer than those reported using dissolving pulp (Henriksson et al. 2008; Iwamoto et al. 2007; Stelte and Sanadi 2009). The fibrillation was conducted using a commercial grinder with a stone disk. This type of mechanical fibrillation method was chosen for its potential for commercial scale-up. Samples were taken periodically throughout the fibrillation process. Morphological appearance of the samples was extensively examined by SEM and TEM to reveal the ultra-fine-structure of CNF that has not been shown in detail in previous studies (Henriksson et al. 2008; Iwamoto et al. 2007; Nakagaito and Yano 2004; Stelte and Sanadi 2009). Time-dependent energy consumption profiles for fibrillation were recorded to investigate the effects of energy input on the degree of polymerization and crystallinity index of the resultant nanofibrils. The goal of this study is to provide a basic understanding of CNF properties to the broad material scientist and nanotechnology research communities for potential large volume and high value utilization.

Materials and methods

Material

Bleached dry lap eucalyptus kraft pulp was obtained from a commercial source (Aracruz Cellulose, Brazil). The pulp was first soaked in deionized water overnight and then disintegrated in a lab disintegrator (TMI, Ronkonkoma, NY) after 10,000 revolutions. The chemical composition of the pulp was: 78.1 ± 1.0 % glucan, 15.3 ± 0.6 % xylan, 0.7 ± 0.1 % Klason lignin, respectively.

Mechanical nanofibrillation

The eucalyptus pulp was fibrillated at suspension solids consistency of 2 % (w/w) using a SuperMass-Colloider (Model: MKZA6-2, Disk Model: MKGA6-

80#, Masuko Sangyo Co., Ltd, Japan) at 1,500 rpm. The SuperMassCollider is equipped with a power meter to record electrical energy input. Two stone grinding disks were positioned on top of each other. The bottom disk rotates while the top one is stationary. Pulp feeding was achieved by gravity. A hydraulic pressure head can also be developed for runs with large capacity when the flow loop is properly constructed. The gap of the two disks was adjusted to - 100 μm from motion zero position after pulp was loaded. The motion zero position was determined right at the contact position between the two grinding disks before loading the pulp. Due to the presence of pulp, there is no direct contact between the two grinding stones even at a negative setting of disk position. Pulp suspension was fed into the disk grinder continuously through a loop consisting of a peristaltic pump (Cole Parmer, Chicago, IL) and plastic tubing. The fibrillated pulp was sampled periodically and time-dependent energy consumption was recorded using a power meter.

Electron microscopy

Specimens for scanning electron microscopy (SEM) were prepared by drying drops of the aqueous slurry on polished aluminum mounts. All SEM samples were sputter-coated with gold to provide adequate conductivity. Samples were imaged and photographed using a Leo EVO 40 SEM. Aqueous fractionated (by centrifuge) and unfractionated CNF samples taken at different fibrillation times were diluted to solids consistency of approximately 0.1 % and analyzed by TEM. Each aqueous sample was adsorbed to freshly glow-discharged carbon-coated grids for 30 s, then rinsed with water and negatively stained with 0.5 % uranyl acetate. Images were recorded on a Hitachi H7650 microscope at 80 kV with a 2 × 2 k AMT CCD camera.

Degree of polymerization and crystallinity index

Viscosity of resulting nanofibrillated cellulose was measured according to TAPPI Standard Method T230 om-99. Degree of polymerization (DP) of nanofibrillated cellulose was calculated by following formula: $DP^{0.905} = 0.75(954 \log(X) - 325)$, where X is viscosity (Mazumder et al. 2000). Crystallinity of nanofibrillated cellulose was measured by a Bruker RFS 1,000 Spectrometer (Bruker Instruments Inc., Billerica, Massachusetts) (Agarwal et al. 2010). The method is based upon the band intensity ratio 380/1096 obtained from the FT-Raman spectrum of the sample.

Fractionation of fibrillated cellulose

An attempt was made to fractionate large network fibrillated cellulose from the small ones using a centrifuge technique (Bai et al. 2009). The fibrillated cellulose sample was first diluted to 0.2 % (w/w). The diluted suspension was continuously stirred for 1 h and then centrifuged at 1,000 rpm for 15 min in a centrifuge (Model 8 K Marathon™, Roter 220.42v01, Fisher Scientific, Pittsburgh, PA). The consistencies of nanofibrillated cellulose before and after centrifuge were determined by a chemical oxygen demand (COD) method (Franson 1985) assuming detected organic materials were $(C_6H_{10}O_5)_n$. Commercial COD test kits (Biosciences, Inc., Bethlehem, PA) were used to digest an aliquot of fibrillated cellulose. COD was measured from the amount of chromium consumed using the spectral intensity of the digested sample at 600 nm, i.e., COD (mg/L) = 3,410.2 × I_{600}. The mass of cellulose can be calculated $m_{C6}H_{10}O_5$(mg/L) = COD/1.185 = 2,877.6 × I^{600} based on calibration.

Results and discussions

Morphological development of cellulose fibrils: SEM examination

The original bleached eucalyptus pulp fibers have an average length of 0.8 mm with an average width of slightly below 20 micrometers as measured by a fiber analyzer (FQA, Optest, Canada). A SEM image of the fibers is shown in Fig. 1. A pulp suspension of approximately 2 % was fed into the SuperMassColloider and was dispersed by centrifugal force into the clearance between the two stone disks and subjected to compressive, shearing and friction forces. Compression forces tend to drive internal fiber fibrillations to break the crosslinks between fibrils and cause fiber delamination (Dekker 2003; Haman 1985; Kerekes 2005). Abrasive shear and friction forces can cause external fibrillation to increase fiber external surface

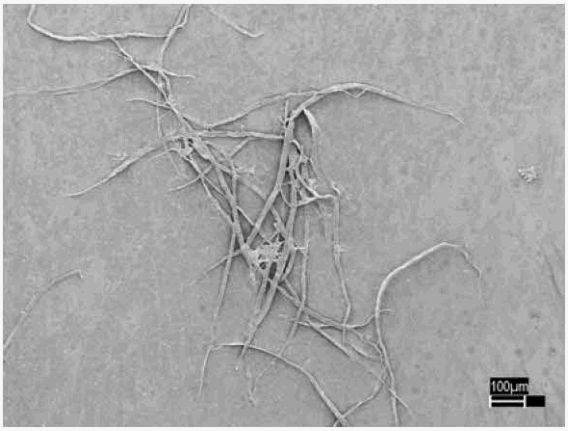

Fig. 1 A SEM image of the unbibrillated bleached eucalyptus pulp (BEP) fibers. Scales = 100 μm.

area by cutting fibers and producing hairs or fibrils from the fiber surface (Hartman 1985; Kerekes 2005), which can be clearly seen in the early stage of milling from SEM imaging (Fig. 2a) The break-up of the cell wall by external fibrillation and delamination of the S2 layer to produce nanofibrils through internal fibrillation are best illustrated in Fig. 2b. Some parts of the cell wall still heald together in some regions while internal fibril delamination occurred where the outer cell wall (can be S1 and P layer was removed The external fibrillanon resulted in cell wall fragments (Fig. 2b). Furthermore, some fragments were from broken P or S1 layers as previously reported using optical microcopy(Uetani and Yano 2011) and may have S2 layer attached (Fig. 2b). This is evidenced

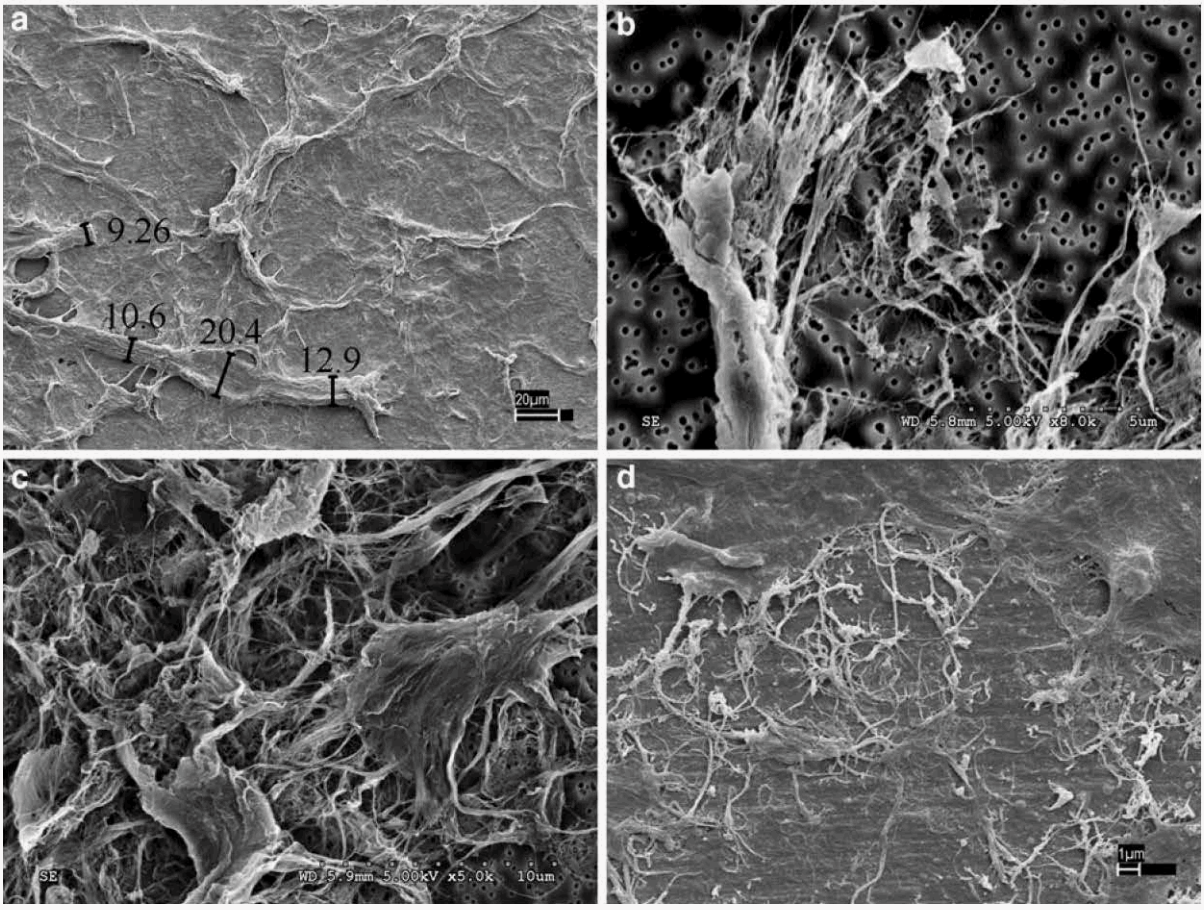

Fig. 2 SEM or FE-SEM images of fibrillated fibers. **a** Fiber breakup, fibrillation time = 0.5 h, scale = 20 μm; **b** FE-SEM: external and internal fibrillation, fibrillation time = 3 h, scale = 5 μm; **c** FE-SEM: cell wall fragment and submicron fibrils, fibrillation time = 3 h, scale = 10 μm; **d** Fibril separation to nanofibrils, fibrillation time = 5 h, scale = 1 μm

from the relatively straight fibrils seen from some cell wall fragments (Fig. 2c). Optical microscopy indicates that fibers with pits can be easily broken into fragments (Uetani and Yano 2011). Eucalyptus, as a hardwood, has a significant amount of vessel elements that are highly pitted, and therefore can be easily fragmented. Internal delamination resulted in separated microfibers or submicron fibrils (Fig. 2b, c) and the separation of the fibrils within the fragments. The microfibers or fibrils can be curled due to latency produced by mechanical shearing (Fig. 2c). The shearing motion can also orient the microfibers or nanofibrils to different directions to cross over as backbones of networks.

Fragmentation and delamination continued as fibrillation proceeded further. Large fragments disappeared, which released nano-sized S1 and P layer fibrils (spiral) and S2 layer fibrils (Fig. 2d). Some highly entangled and partially or completely fibrillated nanofibrils cannot be distinguished under SEM with limited dispersion and resolution; these were examined by TEM.

The formation of nanofibril network TEM examination

SEM imaging focused on examining large structures of fibrillated cellulose. Small or nanoscale cellulose structures are obscured in unfractionated samples and therefore undetectable by SEM due to resolution. TEM imaging can zoom into the nanofibril network to provide clear visualization of ultra-fine morphological development during mechanical fibrillation without concerning the large structure of the fibrillated cellulose. TEM imaging can be subjective and cannot predict whether an observed ultra-fine structure feature is dominant or typical. However, TEM can reveal the details of the entangled micro- or nanofibrils and the "backbone" structural fibrils observed from SEM at low magnifications (Fig. 3a, b). Details of the two nano-scale structures of "backbone" fibrils and the entangled or curled and completely twisted nanofibrils can be seen from Fig. 3b. The image in Fig. 3a was obtained from an unfractionated sample taken after 11 h of fibrillation, showing large sized nanofibril

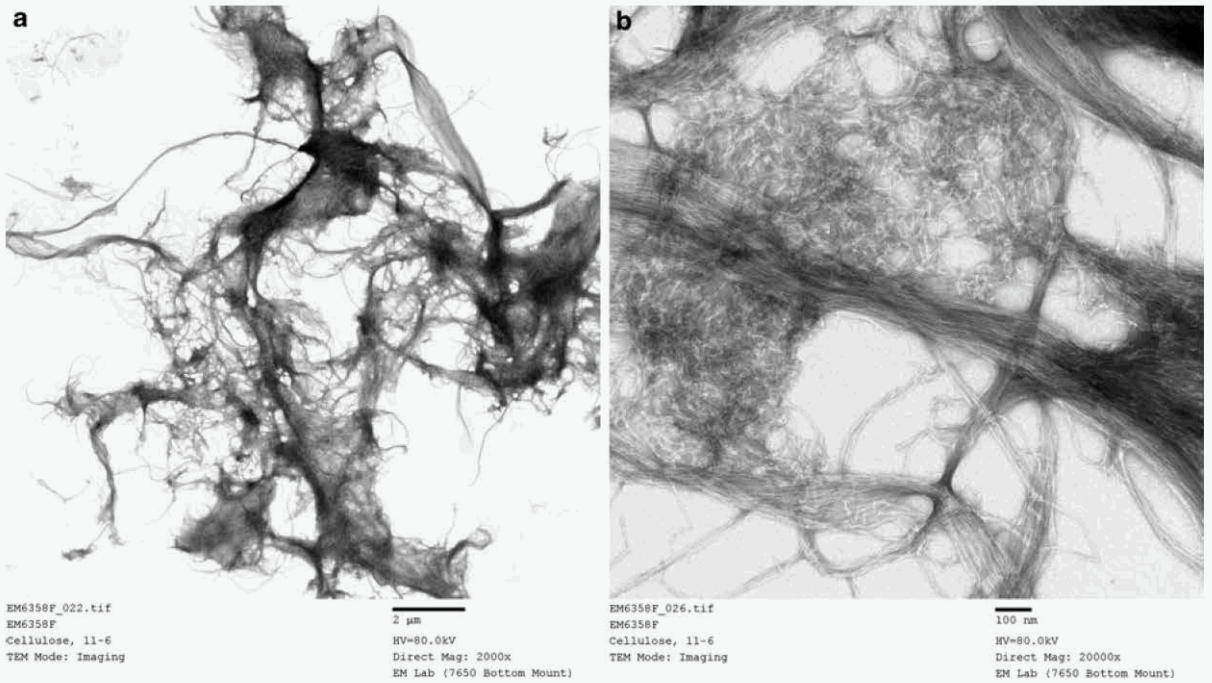

Fig. 3 TEM images of CNF network structure **a** A low magification TEM image of a CNF network, fibrillation time = 11 h, scale = 2 µm; **b** Details of the untwisted backbone fibrils entangles by twisted nanofibrils scale = 100 nm

networks still present even after prolonged mechanical fibrillation. The dimension of Fig. 3a is on the order of 20 μm, the same as the fiber width of the original unfibrillated bleached eucalyptus pulp.

The two main structures produced various ultra-fine features of the CNF network as can be visually described as "tree" (Fig. 4a), "net" (Fig. 4b), "flower" or "torch" (Fig. 4c), "blooming tree'' (Fig. 4d), "ghost" (Fig. 4e), and isolated nanofibril (Fig. 4f). The various morphologies were not necessarily restricted to a particular set of CNF production conditions; multiple features could be potentially found within the same sample. These structural features are described below in detail:

1. The "tree" feature was formed primarily by the internal fibrillation of submicron or large nanofibrils of several hundred nanometers to small nanofibrils of 10-30 nm, and further separation to approximately 5–20nm (Fig. 4a). The small nanofibrils, approximately10 nm, were highly kinked and probably resulted from external fibrillation. The fibril separation caused by internal fibrillation can be better observed from Fig. 5a in which a large nanofibril of approximately 250 nm was separated into 30 nm fibrils and continued separation into 10 nm fibrils. The ultra-fine details of the kinked and naturally helical small nanofibrils can also be better seen from Fig. 5b where separated kinked fibrils at the elemental level of 3–5 nm were present. The length of the shortest segment between two adjacent kinks is on the order of 50–100 nm (Figs. 4a, 5b), approximately equal to the reported length of elemental crystallite, 60 nm (Stamm 1964). This suggests that the shortest segment between two adjacent kinks represents the elemental crystallite of the cellulose, and kinks appeared in the amorphous region of the cellulose chain.
2. The "net" feature was from the cross over backbone fibrils of different scales and the completely twisted and curled nanofibrils that entangled the backbone fibrils (Fig. 4b). The splitting of the backbone fibrils by internal fibrillation to approximately 20-50 nm can also be clearly seen to complicate the net structure. The details of the curled and entangled nanofibrils will be discussed below.
3. The "flower" or "torch" feature was formed by several backbone fibrils on a different scale as the "stem" of the "flower" or the "holder" of the "torch' and the completely entangled and highly twisted and curled nanofibrils (Fig. 4c). The details of the completely entangled and highly twisted and curled nanofibrils can be better observed from Fig. 5c. Partial segmental separation of the elemental fibrils of 3–5 nm between adjacent kinks can be seen. It appears that the unseparated fibrils are also kinked but with relatively less sharp kinks. Furthermore, the segment length between two adjacent kinks is the order of 30–60nm (Fig. 5c), shorter than those observed from the untwisted nanofibrils (Fig. 5b). As a result, the feature appears "soft" and "flower" like. This "soft looking" entangled fibril structure is different from another type of highly entangled, kinked and naturally helical but not twisted nanofibril as may appear in the "tree" feature shown in Fig. 5d. The typical separation between two adjacent kinks is approximately 50–100nm (Fig. 5d), similar to the segment length observed from the unentangled "tree" feature shown in Fig. 4a, and approximately equal to the reported length of the elemental crystallite (Stamm 1964).
4. The "blooming tree'' feature consists of "tree" and "flower" as a "blooming tree". As shown in Fig. 4d, the top part is a "tree" feature with kinked and naturally helical but not twisted nanofibrils and the middle and bottom parts have highly curled and twisted nanofibrils as "flowers". The backbone fibrils serve as tree branches. The image in Fig. 4d indicates that the highly twisted "soft looking" nanofibrils and untwisted and kinked and naturally helical nanofibrils originated from different parts of a fiber cell wall. It is possible that the "soft looking" feature was the released from part of the cell wall with different properties from those backbone fibrils. For example, the P and S1 layers have lower cellulose and higher hemicellulose contents than the S2 layer (Panshin and de Zeeuw 1980), i.e., fibrils in the P and S1 layers are more amorphous than those in the S2 layer. It has been suggested

Fig.4 TEM images show different types of CNF nanostructure. **a** Tree, scale = 500 nm, 3 h: **b** net scale = 500 nm, 7 h **c** flower or torch, scale = 500 nm, 1 h; **d** blooming tree, scale = 500 nm, 7 h: **e** ghost scale = 500 nm, 9 h: **f** single fibril, scale = 500 nm, 7 h

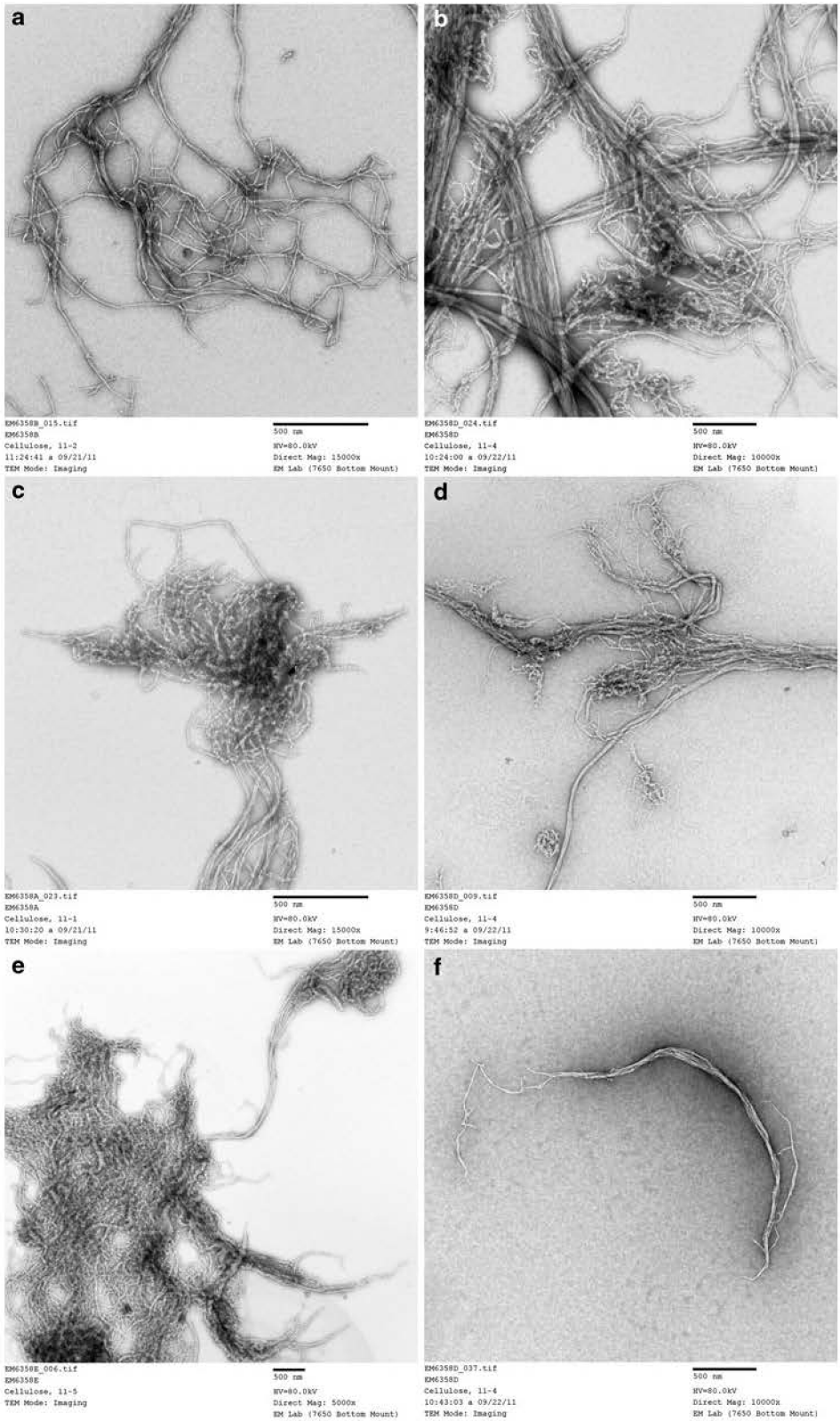
a
EM6358B_015.tif
EM6358B
Cellulose, 11-2
11:24:41 a 09/21/11
TEM Mode: Imaging
500 nm
HV=80.0kV
Direct Mag: 15000x
EM Lab (7650 Bottom Mount)
b
EM6358D_024.tif
EM6358D
Cellulose, 11-4
10:24:00 a 09/22/11
TEM Mode: Imaging
500 nm
HV=80.0kV
Direct Mag: 10000x
EM Lab (7650 Bottom Mount)
c
EM6358A_023.tif
EM6358A
Cellulose, 11-1
10:30:20 a 09/21/11
TEM Mode: Imaging
500 nm
HV=80.0kV
Direct Mag: 15000x
EM Lab (7650 Bottom Mount)
d
EM6358D_009.tif
EM6358D
Cellulose, 11-4
9:46:52 a 09/22/11
TEM Mode: Imaging
500 nm
HV=80.0kV
Direct Mag: 10000x
EM Lab (7650 Bottom Mount)
e
EM6358E_006.tif
EM6358E
Cellulose, 11-5
TEM Mode: Imaging
500 nm
HV=80.0kV
Direct Mag: 5000x
EM Lab (7650 Bottom Mount)
f
EM6358D_037.tif
EM6358D
Cellulose, 11-4
10:43:03 a 09/22/11
TEM Mode: Imaging
500 nm
HV=80.0kV
Direct Mag: 10000x
EM Lab (7650 Bottom Mount)

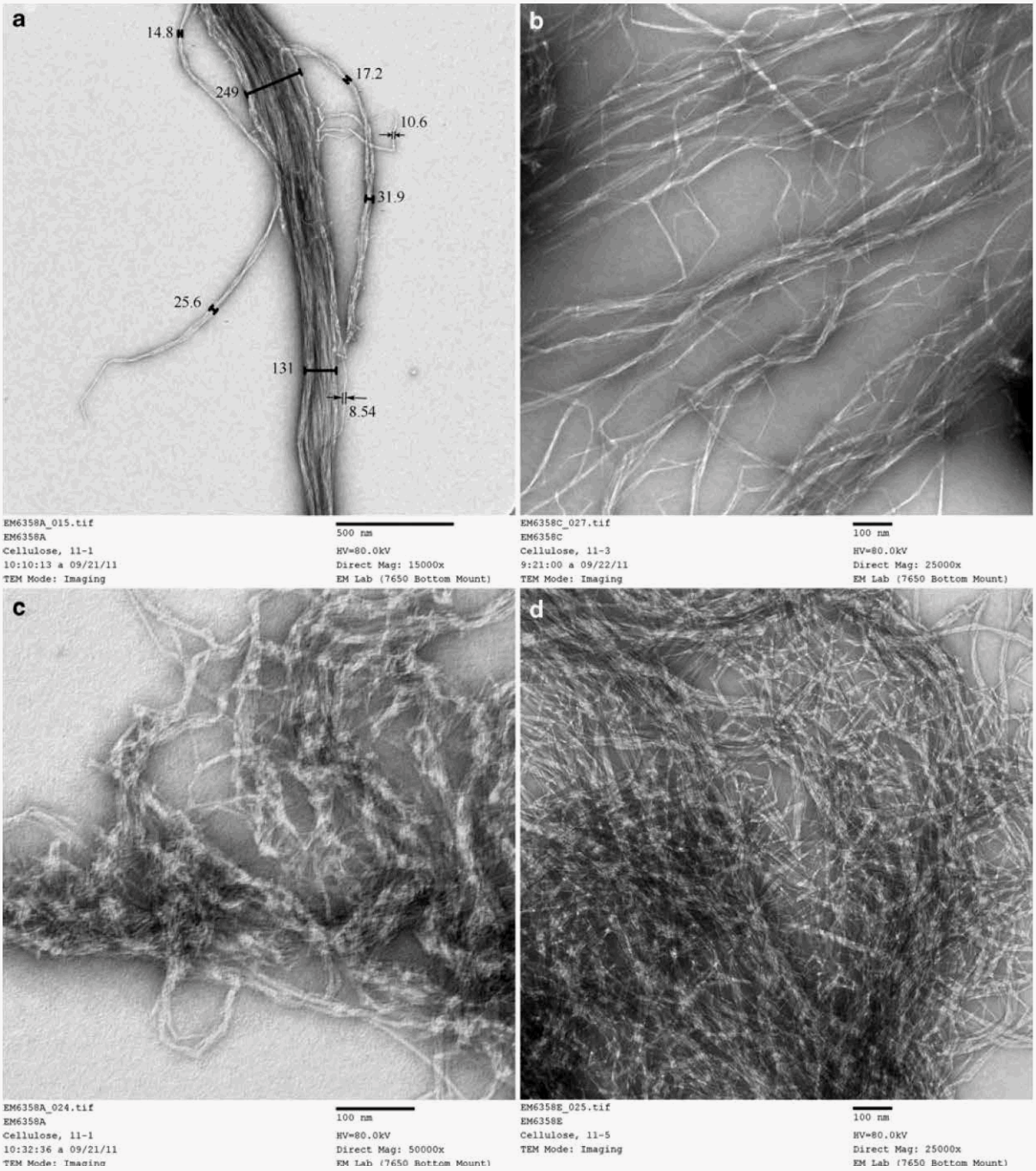

Fig. 5 Details of different nanofibril structures. **a** Splitting nanofibril, scale = 500 nm, 1 h; **b** kinked but untwisted, and not entangled nanofibrils, scale = 100 nm, 5 h; **c** entangled and twisted nanofibrils, scale = 100 nm, 1 h; **d** entangled and kinked but untwisted nanofibrils, scale = 100 nm, 9 h

that variations in fiber cell wall growing conditions induce growth stress, which can affect the orientation of cellulose chains and subsequently crystallization (Stamm 1964). These factors indicate micro or nanofibrils can have different crystallinities. Therefore, it is plausible that the

"soft looking flower" structure may be formed from nanofibrils with large amorphous regions or high hemicellulose content and therefore low average crystallinity, such as those from the P and S1 layers. The "tree" feature and the entangled but untwisted structure shown in Fig. 5d may be from nanofibrils with low hemicellulose content, and therefore with sharper kinks and higher average crystallinity than those "soft looking" fibrils.

5. The "ghost" feature is essentially broken away, highly twisted and entangled "soft looking" nanofibrils from major backbone fibrils (Fig. 4e). Small backbones can still be seen. The image in Fig. 4e also shows a "flower" sticking out of the "ghost" body connected with a small backbone fibril.
6. Isolated stick fibrils are simply broken, untwisted nanofibrils from the network without many kinks, as shown in Fig. 4f. This isolated fibril may be further separated or split into small scales as shown in Fig. 5a, b.

The formation of nanowhiskers: TEM examination

It is very interesting to notice that long duration fibrillation can completely break up the fibril network to result in a very unique nanowhisker structure as shown in (Fig. 6a, b). The nanowhiskers are approximately 250 nm in length and 20 nm in diameter (Fig. 6b). Whiskers made of single elemental fibrils (crystallites), i.e., diameter of 3–5 nm, are also present (Fig. 6b). From the fact that long fibrils appeared in the early stage of whiskerization are not twisted or entangled (Fig. 6a), we hypothesize that the nanowhiskers were derived from the untwisted and naturally helical nanofibrils in Fig. 5b, d, rather than from twisted "soft looking" fibrils shown in Fig. 5c. As discussed in the previous section, the untwisted nanofibrils are stiffer and may be more crystalline, while the twisted "soft looking" fibrils are less stiff and may be more amorphous. Therefore, the nanowhiskers may have high crystallinity. This may prove a mechanical approach to produce cellulose nanocrystals (CNCs).

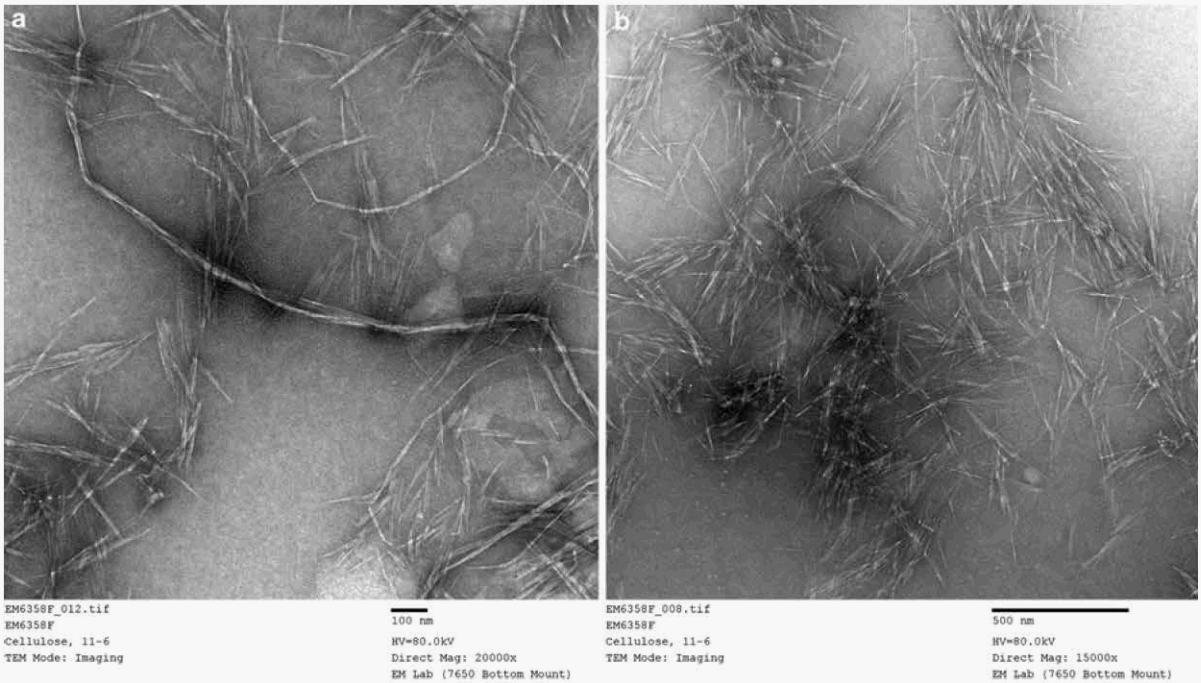

Fig. 6 Nanowhisker structure both obtained at 11 h fibrillation. **a** Early stage of nanowhiskering with the presence of long nanofibrils, scale = 100 nm; **b** nanowhiskers without nanofibrils, scale = 500 nm

Quantitative imaging analysis of cellulose nanofibrils and nanowhiskers

Quantitative imaging analyses were conducted using Image-Pro Plus software (Media Cybernetics, Silver Spring, USA) to determine the diameters of nanofibrils and the lengths of the nanowhiskers. Seventy-one (71) and 161 diameter measurements and 51 length measurements were manually taken from the images shown in Figs. 2d, 4a and 6b, respectively. The distribution of fibril diameter and whisker length were calculated and shown in Fig. 7a–c, respectively. The results indicated that SEM imaging is only able to resolve large fibrils with a diameter of 100 nm or more (Fig. 7a), while TEM imaging can resolve nanofibrils tens of nanometers in diameter and even elemental fibrils of 3–5 nm in diameter (Fig. 7b). The lengths of the nanowhiskers are on the order of several hundred nanometers (Fig. 7c). The lengths of short nanowhiskers are approximately equal to the reported length of single cellulose crystallite of 60 nm (Stamm 1964). This supports the hypothesis that the nanowhiskers (Fig. 6a, b) are highly crystalline.

CNF fractionation by centrifuge

Increased fibrillation time tends to reduce the size of the of CNF structure in general. For example, the nanowhisker structure shown in Fig. 6a, b was observed from a sample fibrillated for 11 h. However, large sized CNF structures still exist even after prolonged fibrillation. For example, the large network structure shown in Fig. 3a was from a sample taken after 11 h of fibrillation. Operators of TEMs can sometimes selectively look for certain features, which makes quantitative analysis of morphological features, such as size, unreliable and biased. When comparing all TEM images of a supernatant fraction with the corresponding precipitated fraction derived from centrifugation at $200\times g$, it appears that relatively more isolated fibrils were observed from the supernatant fraction than in the precipitated fraction. This suggests that the results from centrifugation may be used as one way to quantitatively characterize the size of the CNF network. We correlated the electrical energy input to the SuperMassColloider to the fraction of the supernatant of total CNF. The results indicate that the supernatant fraction increased almost linearly with fibrillation energy and then reaches an

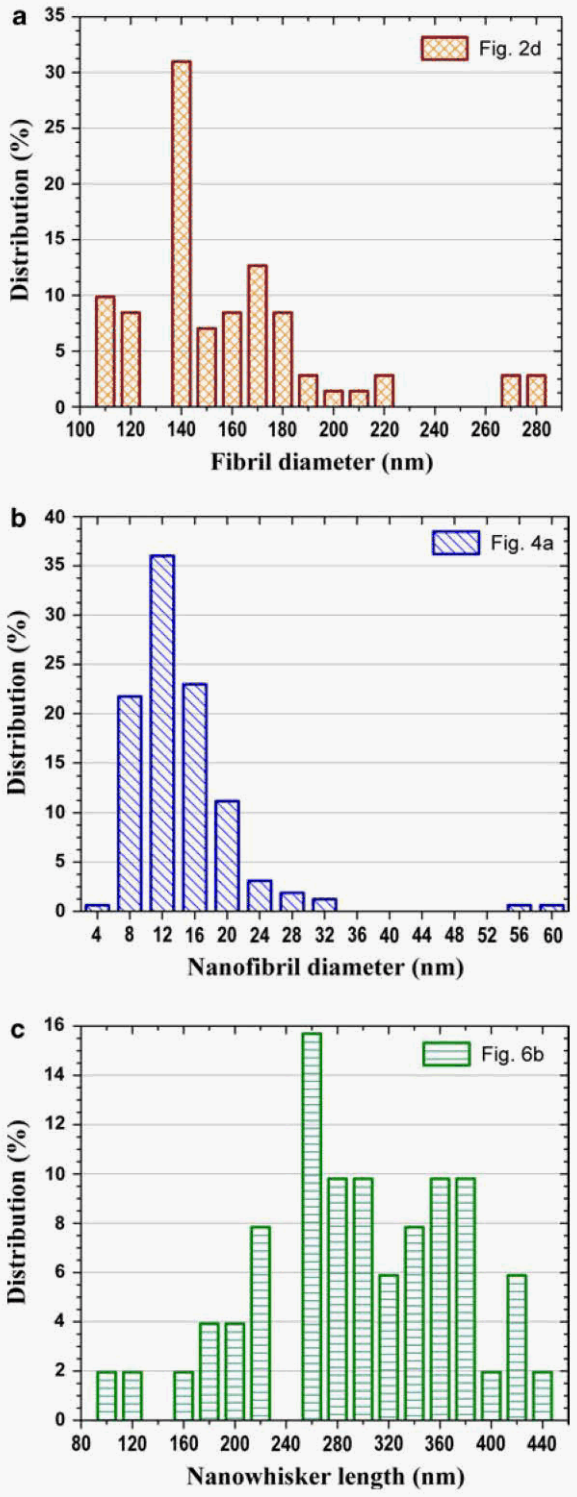

Fig. 7 Distributions of fibril diameters and nanowhisker length from imaging analyses. **a** From Fig. 2d: **b** from Fig. 4a: **c** from Fig. 6b

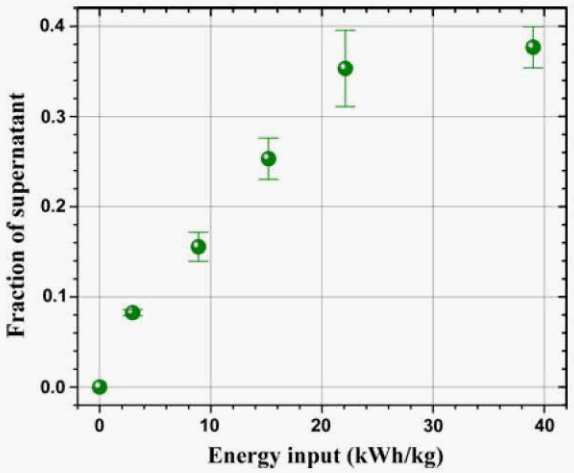

Fig. 8 Effect of electric energy input on mass fraction of CNF in the supernatant

asymptotic value of approximately 40 % (Fig. 8). This suggests that the effectiveness of nanofibrillation for the given grinder and disk pattern has reached its limit. Further studies need to be carried out using different CNF samples as well as different centrifuge conditions to examining the validity of this approach for CNF size characterization.

Effect of energy input on physico-chemical properties of CNF

Electric energy consumption for fibrillation was found to increase almost linearly with fibrillation time as shown in Fig. 9. The amount of energy consumed was comparable with the data reported in the literature (Siró and Plackett

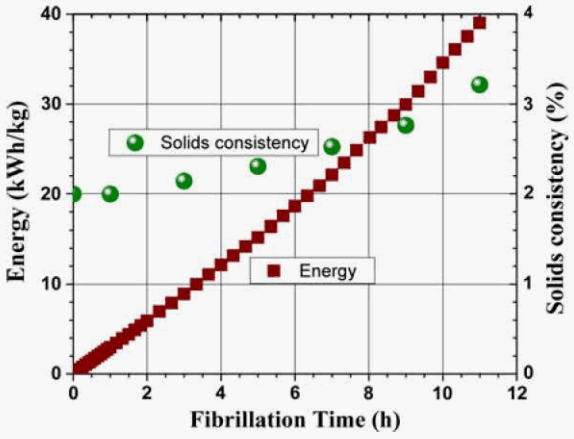

Fig. 9 Time-dependent cumulative electric energy consumption and CNF pulp suspension consistency

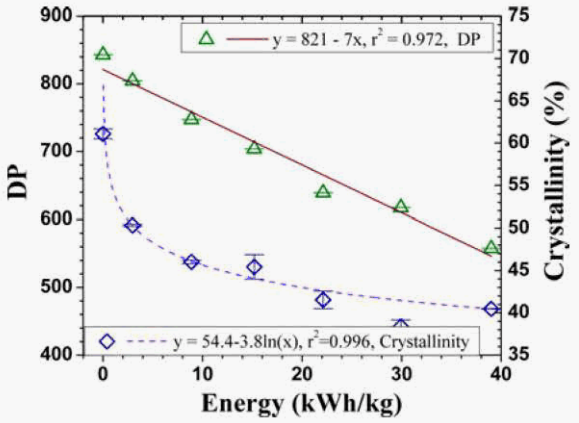

Fig. 10 DP and crystallinity index of nanofibrillated cellulose as a function of electric energy input

2010). The results suggestthat nanocellulose production is very energy intensive and on the order of 5-40 kwh/kg when using bleached pulp by direct mechanical fibrillation. Heat generated by friction during fibrillation evaporated water, resulting in an increase in cellulose suspension consistency from the initial value of 2 to 3.2 % after 11 h (Fig. 9). The increase in solids consistency increased specific fibrillation energy as can be seen from the increased slope of time-dependent electric energy consumption curve (Fig. 9).

Degree of polymerization (DP) and crystallinity are the two most important physico-chemical properties of nanofibrillated cellulose. Mechanical grinding physically destroyed cellulose crystals and broke cellulose chains, resulting in small crystals with short chain length. The DP of the fibrillated cellulose decreased linearly with electric energy input from approximately 850 to 550 after 11 h of mechanical fibrillation. The crystallinity decreased rapidly initially from 62 to 50 with fibrillation and continued to decrease slowly to approximately 40 (Fig. 10).

Conclusions

A bleached eucalyptus pulp was mechanically fibrillated to nanocellulose using a commercial stone grinder at an electrical energy input between 5 and 30 kWh/kg Mechanical shearing and compression motions produced external and internal fibrillation, respectively, to break up the fiber cell wall into fragments as well as fines or microfibers on the order of 1-10 µm. Continued fibrillation resulted in further fragmentation of the cell wall

and separation of microfibers, which produced micro and nanofibrils at scales of submicron, hundred, tens, and even a few nanometers—elemental fibrils. The resultant cellulose nanofibril (CNF) networks have two major structures: (1) highly kinked, naturally helical, but not twisted fibrils. Shearing motion disoriented these untwisted fibrils as backbones of CNF networks. (2) "soft looking" fibrils to completely entangle the fibril network. These fibrils are highly twisted and curled (or less distinctively kinked). The backbone and "soft looking" fibrils appears in different features of a CNF network, such as "tree", "flower" or "torch", "blooming tree", "ghost", etc. The untwisted nanofibrils may be originated from stiff or relatively crystalline cellulose with very small amorphous regions, such as the S2 layer with low hemicellulose content, while the twisted "soft looking" fibrils may be from the outer layers with relatively low cellulose and high hemicellulose content and large amorphous regions. A unique nanowhisker structure was also observed after prolonged fibrillation. It appears the nanowhiskers resulted from the untwisted nanofibrils and are more crystalline.

The bulk CNF network size gradually decreased with mechanical fibrillation time. As a result, centrifuging can statistically fractionate small nanofibril networks from large ones. Furthermore, the average DP and crystallinity index of the fibrillated cellulose decreased with fibrillation time and energy input.

Acknowledgments We acknowledge the financial supports by a USDA Agriculture and Food Research Initiative (AFRI) Competitive Grant (No. 2011-67009-20056) and Chinese Scholarship Council (CSC). The funding from these two programs made the visiting appointment of Wang at the USDA Forest Products Laboratory (FPL) possible. We also acknowledge Ann Masco of FPLL Paper Test Lab for FQA analysis. The authors also wish to thank Anne Kamata, SAIC-Frederick Inc. for electron microscopy imaging. TEM imaging work was funded in whole or in part with federal funds from the National Cancer Institute, National Institutes of Health, under Contract No. HHSN261200800001E. The content of this publication does not necessarily reflect the views or policies of the Department of Health and Human Services, nor does mention of trade names, commercial products, or organizations imply endorsement by the US Government.

References

Agarwal UP, Reiner RS, Ralph SA (2010) Cellulose I crystallinity determination using FT-Raman spectroscopy: univariate and multivariate methods. Cellulose 17(4):721–733

Bai W, Holbery J, Li K (2009) A technique for production of nanocrystalline cellulose with a narrow size distribution. Cellulose 16(3):455–465

Dekker J (2003) New insights in beating leading to innovative beating techniques. 7th PIRA International Refining Conference, Stockholm, Sweden

Eichhorn SJ, Dufresne A, Aranguren M, Marcovich NE, Capadona JR, Rowan SJ, Weder C, Thielemans W, Roman M, Renneckar S et al (2010) Review: current international research into cellulose nanofibres and nanocomposites. J Mater Sci 45(1):1–33

Franson MH (1985) Standard methods for the examination of water and wastewater, 16th edn. American Public Health Association (APHA), Washington, DC, pp 532–537

Habibi Y, Lucia LA, Rojas OJ (2010) Cellulose nanocrystals: chemistry, self-assembly, and applications. Chem Rev 110(6): 3479–3500

Hartman RR (1985) Mechanical treatment of pulp fibers for paper property development. In: Punton V (ed) Mechanical Engineering Publications Limited, Oxford, England, pp 413–442

Henriksson M, Berglund LA, Isaksson P, Lindström T, Nishino TD (2008) Cellulose nanopaper structures of high toughness. Biomacromolecules 9:1579–1585

Iwamoto S, Nakagaito AN, Yano H (2007) Nano-fibrillation of pulp fibers for the processing of transparent nanocomposites. Appl Phys A Mater Sci Process 89:461–466

Iwamoto S, Abe K, Yano H (2008) The effect of hemicelluloses on wood pulp nanofibrillation and nanofiber network characteristics. Biomacromolecules 9(3):1022–1026

Kerekes RJ (2005) Characterizing refining actions: linking the process to refining results. 8th PIRA International Refining Conference, Barcelona, Spain

Klemm D, Kramer F, Moritz S, Lindstrom T, Ankerfors M, Gray D, Dorris A (2011) Nanocelluloses: a new family of nature-based materials. Angew Chem Int Ed 50(24):5438–5466

Law KN, Lo SN, Valade JL (1985) Beating behavior of sulphite-mechanical hardwood pulps. Pulp Paper Canada 86(1): 70–74

Marton R, Goff S, Brown AF, Granzow S (1979) Hardwood TMP and RMP modifications. TAPPI 62(1):49–53

Mazumder BB, Ohtani Y, Cheng Z, Sameshima K (2000) Combination treatment of kenaf bast fiber for high viscosity pulp. J Wood Sci 46(5):364–370

Nakagaito AN, Yano H (2004) The effect of morphological changes from pulp fiber towards nano-scale fibrillated cellulose on the mechanical properties of high-strength plant fiber based composites. Appl Phys A Mater Sci Process 78:547–552

Pääkkö M, Ankerfors M, Kosonen H, Nykänen A, Ahola S, Österberg M, Ruokolainen J, Laine J, Larsson PT, Ikkala O et al (2007) Enzymatic hydrolysis combined with mechanical shearing and high-pressure homogenization for nanoscale cellulose fibrils and strong gels. Biomacromolecules 8(6):1934–1941

Panshin AJ, de Zeeuw C (1980) Textbook of wood technology. McGraw-Hill Book Company, New York

Saito T, Hirota M, Tamura N, Kimura S, Fukuzumi H, Heux L, Isogai A (2009) Individualization of nano-sized plant cellulose fibrils by direct surface carboxylation using TEMPO

catalyst under neutral conditions. Biomacromolecules 10(7): 1992–1996

Siró I, Plackett D (2010) Microfibrillated cellulose and new nanocomposite materials: a review. Cellulose 17:459–494

Siró I, Plackett D, Hedenqvist M, Ankerfors M, Lindström T (2011) Highly transparent films from carboxymethylated microfibrillated cellulose: the effect of multiple homogenization steps on key properties. J Appl Polym Sci 119(5): 2652–2660

Stamm AJ (1964) Wood and cellulose science. The Ronald Press Company, New York, p 549

Stelte W, Sanadi AR (2009) Preparation and characterization of cellulose nanofibers from two commercial hardwood and softwood pulps. Ind Eng Chem Res 48(24):11211–11219

Tejado A, Alam MN, Antal M, Yang H, van de Ven TGM (2012) Energy requirements for the disintegration of cellulose fibers into cellulose nanofibers. Cellulose 19(3): 831–842

Turbak AF, Snyder FW, Sandberg KR (1983) Microfibrillated cellulose, a new cellulose product: properties, uses, and commercial potential. J Appl Polymer Sci; Appl Polym Symp 37:815–827

Uetani K, Yano H (2011) Nanofibrillation of wood pulp using a high-speed blender. Biomacromolecules 12(2):348–353

Wegner TH, Jones EP (2009) A fundamental review of the relationships between nanotechnology and lignocellulosic biomass. In: Lucia LA, Rojas OJ (eds) The nanoscience and technology of renewable biomaterials, 1 st edn. Wiley, New Jersey, pp 1–41

Zhu JY, Sabo R, Luo X (2011) Integrated production of nanofibrillated cellulose and cellulosic biofuel (ethanol) by enzymatic fractionation of wood fibers. Green Chem 13(5):1339

Zimmermann T, Pöhler E, Geiger T (2004) Cellulose fibrils for polymer reinforcement. Adv Eng Mater 6(9):754–761